



### **Science Arts & Métiers (SAM)**

is an open access repository that collects the work of Arts et Métiers Institute of Technology researchers and makes it freely available over the web where possible.

This is an author-deposited version published in: <https://sam.ensam.eu>  
Handle ID: <http://hdl.handle.net/10985/23272>

#### **To cite this version :**

Asma BOUMEDINE, Samir LECHEB, Khaled BENFRIHA, Pascal OMNES - Investigating the effect of process parameters for fused filament fabrication - Progress in Additive Manufacturing - 2023


Any correspondence concerning this service should be sent to the repository

Administrator : [scienceouverte@ensam.eu](mailto:scienceouverte@ensam.eu)



---

# Investigating the effect of process parameters for fused filament fabrication

Asma Boumedine<sup>1,2</sup>  · Samir Lecheb<sup>2</sup> · Khaled Benfriha<sup>1</sup> · Pascal Omnes<sup>3,4</sup>

## Abstract

Fused Filament Fabrication (FFF) is a promising technology that is largely developed in small series, as this technology optimizes supply chains by reducing production time and costs. However, its shortcomings have slowed its adoption as a dominant production technology. Among its weaknesses, this work focuses on geometric and dimensional accuracy within tolerance range. There is a need for understanding the sources of geometrical inaccuracies and for methods of characterizing them, in order to modify the input parameters to eventually obtain the desired geometry. This work first focuses on the geometric and dimensional accuracy of parts printed by the FFF process by studying the influence of the inner radius of a cylindrical part, the type of material and the type of filling pattern. The levels with the greatest dimensional dispersion are the largest radius, the nylon material, and the hexagonal filling pattern. Secondly, a defect characterization method associated with a parametric mathematical model is developed. The 3D scanner enables the retrieval of the coordinates of the printed geometry; this allows to characterize the errors with respect to the theoretical 3D model and to modelize the printed part by a series of ellipses of which we obtain the analytical equations, as a first step of a correction process.

**Keywords** Additive manufacturing (AM) · Fused Filament Fabrication (FFF) · Design of experiment (DOE) · Full factorial design · Dimensional accuracy · Composites · Mathematical modelling · Geometrical characterization

## 1 Introduction

Additive manufacturing (AM) or prototyping is a revolutionary technology which allows fabricating 3D components based on CAD model data [1–3]. This sophisticated concept of product design and manufacturing allows it to become the third industrial revolution [4]. This particular way of production makes it possible to manufacture complex models [5–7]. Versatile design, and with a large selection of materials, these are features that fall within its scope of application [8]. In the parts there are three types of active functional surfaces (relative movement, guidance), passive functional surfaces (assembly), enveloped surfaces (structure). High precision is necessary for functional and active surfaces. Today, in order to obtain functional precision, the parts are retouched in machining on functional surfaces. The purpose of the work is to enable to qualify the components geometrically, in order to allow in a second phase to correct the manufacturing parameters, Thus up to a certain level of accuracy. The aim is to be able to use more 3D printed parts that comply with the functional specifications as soon as 3D printing is completed, the process can thus be better

---

✉ Asma Boumedine  
a.boumedine@univ-boumerdes.dz;  
asma.boumedine@ensam.eu

Samir Lecheb  
S.lecheb@univ-boumerdes.dz

Khaled Benfriha  
khaled.benfriha@ensam.eu

Pascal Omnes  
pascal.omnes@cea.fr

<sup>1</sup> Arts Et Métiers Institute of Technology, LCPI, HESAM University, 75013 Paris, France

<sup>2</sup> Faculté de Technologie, LDMV, University of M'Hamed Bougara 3500, Boumerdes, Algeria

<sup>3</sup> Service de Thermo-Hydraulique Et de Mécanique Des Fluides, Université Paris-Saclay, CEA, 91191 Gif-Sur-Yvette, France

<sup>4</sup> Institut Galilée, Université Sorbonne Paris Nord, LAGA, CNRS UMR 7539, 99 Av. J.-B. Clément, 93430 Villetaneuse, France

exploited directly in more critical areas such as healthcare and aerospace where dimensional and geometric accuracy of components is fundamental. AM methods are classified into seven different categories, according to the American Society for Testing and Materials (ASTM) standards: Binder Jetting, Powder Bed Fusion, Directed Energy Deposition, Material Jetting, Material Extrusion, Sheet Lamination, and photopolymerization [9, 10]. Several materials were developed for AM, proper to each process. For instance, metals and hybrid metals are used for the deposition of Directed Energy, photopolymers for the jet of materials, and thermoplastics for the extrusion process [11]. The polymers used are in filaments form, such as acrylonitrile butadiene styrene (ABS), polyethylene (PE) or polylactic acid (PLA), polyamide (PA or Nylon) [12]. Pure polymers do not achieve the characteristics of composites, while the objective of the industries is to have stronger and lighter materials [13]. In order to achieve the desired mechanical properties, suitable reinforcement is added to the polymer matrix [14]. This method was undertaken by MarkForged® (Cambridge, MA, USA); it is based on inserting continuous fiber reinforcement into the 3D model via the second nozzle, the first extruder being for the polymer matrix. Dickson et al. investigated the influence of continuous glass, carbon and Kevlar fibers using the fused deposition modelling method; they evaluated the mechanical performance in tension and flexure. They found that parts fabricated using carbon fibre yielded the largest increase in mechanical strength and identified which percentage of fiber content provides the maximum efficiency [15]. The study of Justo et al. focuses on the experimental characterization of nylon-based composite coupons; they found a significant improvement in mechanical properties over un-reinforced nylon parts, although the process requires an upgrade to obtain proper compaction of the material [16].

The quality of parts produced by the FFF process is a function of material, part geometry, and process parameters [17]. Most of optimization research in extrusion systems concentrated on process parameters such as temperature of extrusion, filling velocity, raster angle, diameter of nozzle, temperature of envelope, layer thickness. The effect of filling pattern was also investigated; Fernandez-Vicente et al. have studied the effects of filling patterns and filling percentage on the tensile strength of ABS printed parts. The maximum tensile strength is attained in a rectilinear configuration with a 100% infill percentage [18]. Baich et al. studied the impact of different types of filling patterns on the cost and strength of printed components. It is an aid to the decision for parts mechanically solicited; it turns out that on entry of range printers, it is more interesting to fill parts completely [19]. The effect of infill pattern on tensile and flexural strength and modulus of components produced by the FFF process was investigated experimentally by Akhoundi et al. The studied input parameters were infill percentage (20, 50,

100%) and infill pattern types including rectilinear, concentric, Hilbert curve and honeycomb. The required flexural and tensile behaviours were with the concentric infill at all the indicated infill percentages [20]. Maurya et al. examined the effect of infill pattern and infill density on the printing time and dimensional accuracy of FDM 3D printed cubes; the results showed that the maximum dimensional inaccuracy on the sides of the cubes is found to be 0.95%; also, increasing the sample's infill density increases the time it takes to print it and also increases the volume error [21]. Alafaghani et al. examined the influence of FDM printing conditions on the final component's mechanical properties and dimensional accuracy; the repeatability and resulted tolerances compared to 3D CAD model were also investigated. It was shown that building direction, extrusion temperature, and layer height significantly affect the mechanical properties. Using larger specimens with lower filling percentages emphasizes the influence of filling patterns [22].

Many complexities occur in AM; it could be hierarchical complexity, complexity of materials, complexity of forms as well as functional complexity of free form designs [23, 24]. Even though, this process is widely used but still necessitates upgrading in geometrical accuracy and dimensional exactitude, repeatability and associated tolerances [25], and also in shear and tensile strength, as well as in surface quality [26]. The associated inaccuracy of the surface shape and structure and of the entire geometry is an impediment for the deployment of AM in critical industries [27, 28], where precision is required [29]. Of these issues, accuracy and precision are impediments which prevent AM from becoming a primary production process [30]. To extend the use of AM and increase scalability, it is mandatory to understand the source of error generation to obtain optimal products [31], but also to propose approaches to compensate these errors. A preliminary step for this is to characterize the geometry of the parts that are actually printed by a given printer.

On the one hand, several researchers have dealt with the problem of dimensional accuracy and precision in the AM process. Mahesh et al. have assessed the performance of rapid prototyping systems by incorporating a critical geometric feature into the initial component (reference) to quantify the geometric accuracy [32]. Weheba and Sanchez-Marsa determined the optimal process parameters in SLA process by considering deviations of diameter measurements from the given CAD values, flatness, and surface finish [33]. Bochmann et al. investigated the origin of imprecision in FFF with considering accuracy and surface quality [31]. El-Katatny et al., measured and analyzed error generation in FFF process; they specifically considered the error related to geometric characteristics of specific markers on anatomical parts [34]. Tootooni et al. [35, 36] and Rao et al. [37] used spectral graph theory methodology to quantify the geometric precision of components produced by FFF process.

Garg et al. analyzed the effect of process parameters including Layer Thickness (LT), Infill Density (ID), and Printing Speed (PS) on the dimensional accuracy of cylindrical pin part fabricated by FFF process. Based on the design of experiment and analysis of means (ANOM) diagrams and Response surface methodology optimization [38].

On the other hand, some components manufactured with 3D printing provide functions requiring critical geometric characteristics; this is the case in particular, for guidance systems, where a means of rapid characterization is necessary before installation. This has the triple objective of identifying geometric and dimensional defects, validate or invalidate the part, and allow the modification of the 3D machine programming parameters regarding to correct errors. For this, there are complex numerical characterization methods based on the work of [39–45]. A review of approaches developed to model and predict shape deviations and to improve geometric quality of printed parts [46].

Regarding these two aspects, the aim of this work is twofold: First, we investigate the effect of the following three process parameters: radius size, material type and filling pattern, on the dimensional accuracy of 3D printed FFF cylindrical parts using full factorial design of experiment (DOE). To our knowledge, the effects of this specific combination of these three parameters has not been investigated before. Secondly, this work makes it possible to meet a simple and efficient diagnostic requirement necessary for the rapid manufacture of parts. It proposes to characterize each layer (section) of the 3D printed cylinder by an ellipse. The research objectives are to analyse the deviation between the large and small axes as a measure of cylindricity. More precisely, from the coordinates of a set of points in each section, we find the ellipse passing as close as possible to the given coordinates. The analysis of the superimposed succession of ellipses allows characterizing the manufactured part in a simple and efficient way. The analytical expression of these ellipses will be the first step in a future attempt to correct the instructions given to the printer, so that it eventually prints a cylinder as close as possible to the desired geometry.

The remainder of this paper is organized as follows: Sect. 2 introduces the methodology of this research, materials, and processing. Section 3 describes the experimental measurement procedure and FFF processing conditions, Sect. 4 analyses the DOE results, Sect. 5 presents the approach to obtain the equation of the ellipse that is closest to a given set of measured points on the printed part, and finally Sect. 6 highlights the conclusions of this study.

## 2 Methodology

In this work the FFF technique is adopted, the process is based on the deposition of successive layers of molten material on the build plate through a heated nozzle according to 3D computer-aided design (CAD) data [47, 48]. In the FFF process the fabrication of the 3D component passes through many steps. Figure 1 shows the general 3D printing process from the modeling to the final product.

General flow of 3D printing process.

### 2.1 Materials and processing

The physical base (sample) of the studied model is a cylinder shown in Fig. 2 with fixed thickness and height of  $e = 10$  mm and  $h = 40$  mm respectively. The variable geometric parameter is the inner radius:  $r_1 = 5$  mm,  $r_2 = 10$  mm,  $r_3 = 15$  mm. The raw material is polyamide 6 (PA 6), which is presented

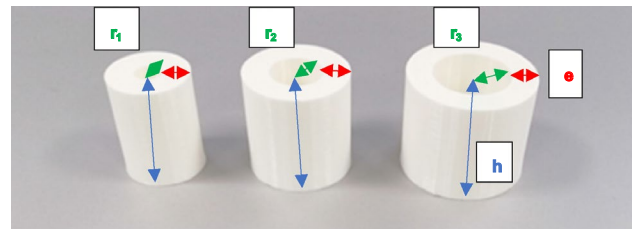


Fig. 2 Model part (sample)

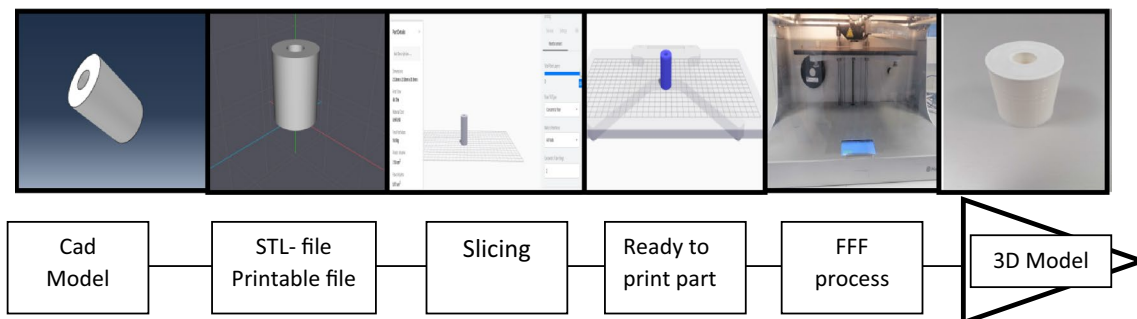


Fig. 1 Flow chart of 3D printing process

as one of the most recent matrix materials for the manufacture of composite parts with Markforged® 3D printers. For the reinforcement, two types of filling were chosen: carbon fiber and glass fiber.

In the current study, the FFF technique using the Mark Two™ Markforged® 3D printer was used to fabricate the samples. It is a Bi-material machine equipped with a double extrusion, one for the effective matrix and one for the continuous fiber. It allows printing composite parts by combining matrix materials (Onyx, Nylon) with reinforcement fibers, see Fig. 3 (a) (Glass fiber, Carbon fiber). The printing process of Markforged® 3D printer is presented in Fig. 3 (b). As shown in this figure, the feeding mechanism of fibers and matrix is furnished with two nozzles.

### 2.1.1 Geometric accuracy measurement

The 3D scanner (Solutionix D500) makes it possible to scan the 3D printed geometry and obtain the coordinates of the point cloud.

The dimensional calculation was performed by the 3D Geomagic® Control X™ software. It calculates the geometric deviations between the measured 3D printed sample and the computer-aided design (reference model). A pre-processing shown in Fig. 4 (3), then the mathematical resolution (Sect. 5) allows to characterize the printed part.

## 3 Experimental procedure

### 3.1 Printing conditions

The geometry of the 3D printed specimens was modeled using Solidworks, exported as an STL file to the 3D printing software. The nylon (PA 6) and fiber layers were printed at a hot end temperature of 273 and 232 °C, respectively. Carbon fiber was printed in layers of 0.125 mm and glass fibers were printed in layers of 0.1 mm. The machine allows placing the fibers in the desired orientation on the layer-by-layer deposition process, two types of samples have been considered: unreinforced and continuous reinforced nylon samples. For

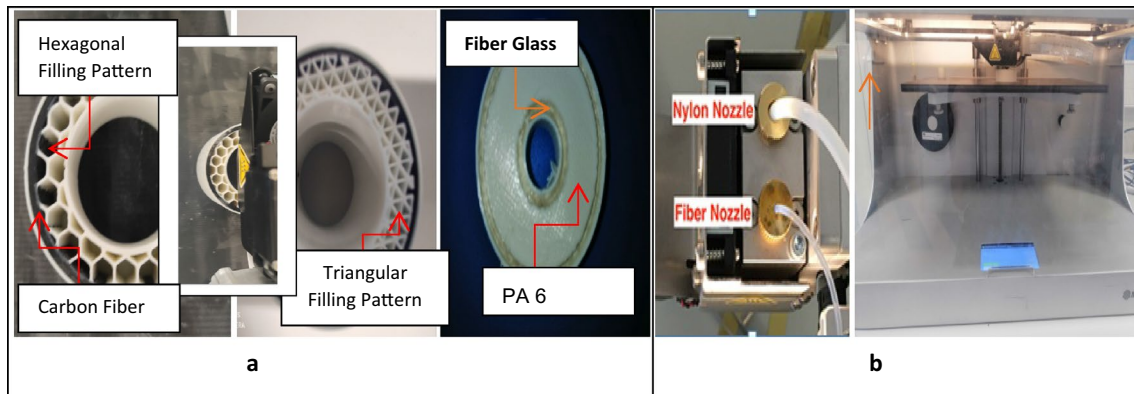


**Fig. 3** a Continuous fiber reinforced composites (exp: Carbon fiber and Glass fiber) and b Markforged® 3D printing process.

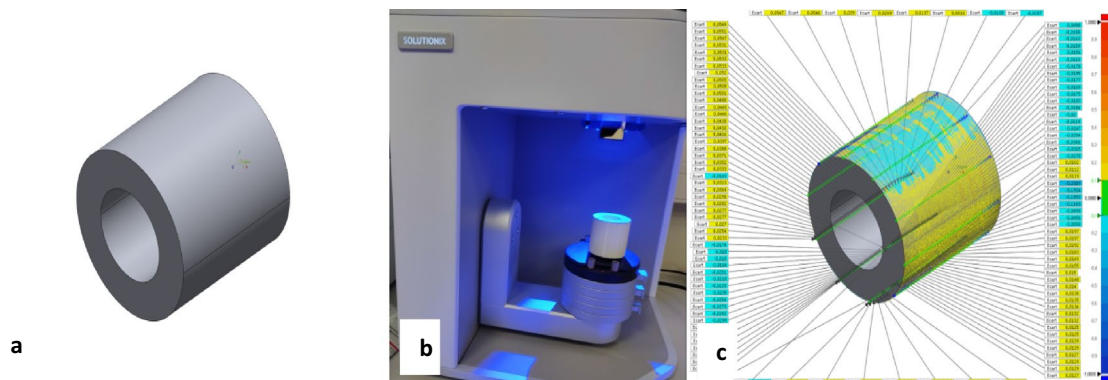


**Fig. 4** The followed methodology steps: a design phase, b Scan and 3D point cloud recovery, c geometric deviations recovery by comparing the CAD model and the 3D printed part



both nylon (polymer) and composites components, the filling patterns used are triangular, rectangular, and hexagonal.

### 3.2 Selection of process parameters

Literature study [17–22] shows that the following three impact factors are influential in the FFF process: inner radius size, material type and filling pattern, and so we have chosen them for the DOE. Moreover, the combination of these three parameters has not been investigated before. On the other hand, these factors are representative of most cylindrical parts printed in 3D. Thus, in this research, a complete three-level factorial design was applied. The experimental design matrix, an L9 ( $3^3$ ), with 27 runs was chosen to account for the factors and their levels as shown in Table 1.

## 4 Statistical analysis of impact factors

The objective is to investigate the relationship between the input parameters (impact factors) and the output response (dimensional deviation). Analysis of variance (ANOVA) was performed using the Minitab 17 [49]. ANOVA reports are described in Annexes 7.2 and 7.3.

### 4.1 Analysis of the input factors on the average deviation

#### 4.1.1 Analysis of normalized effects

The objective of the analysis of normalized effects is to determine whether a factor or a combination of factors has a significant influence on dimensional accuracy. Figure 5 (a) shows the Pareto plot of normalized effects for the mean deviation, in which the probability of rejecting the null hypothesis ( $\alpha$ ) was set to '0.05'. The B factor (material type) and the BC combination (material type /filling pattern) show the highest and lowest values of the normalized effects, respectively. This means that B was rated as the factor most related to the mean dimensional deviation, while the combination BC was rated as the least related factor. In addition, the critical normalized effect was calculated to be 2.306. The normalized effects of the combinations AB, AC, BC and C (filling pattern) are less than 2.306, which means

that these four factors and combinations affect less the average dimensional deviation.

#### 4.1.2 Main effects for the average deviation

The system generates parts that are on average smaller than the CAD, this is especially true for pure nylon material, while parts are in average larger for the nylon material reinforced with carbon fibers and fiberglass (Center picture in Fig. 5 (b)). The reinforcement fibers likely prevented thermal shrinkage.

- The radius size and the filling pattern have little influence on the measurements because they are all close to the average value.
- The radius for which printed parts are closest to the CAD model is  $r = 10$  mm.
- Nylon reinforced with carbon fiber is classified as the best material because it is more accurate.
- The hexagonal filling pattern is considered as the most accurate filling pattern.

#### 4.1.3 Interactions for the mean deviation (adjusted means)

The observation in Fig. 5 (c) shows the non-linearity of the curves corresponding to different types of material and infill patterns. For the analysis of the correlation between the radius size and the type of material, it is observed that, for a radius value of 15 mm, the maximum average value is reached with nylon, but this is not true anymore for the other two materials.

For the nylon material reinforced with glass fibers, the results obtained are similar to those reinforced with carbon fibers with a lower deviation.

For the combination (radius, filling pattern), we observe a strong interaction manifested by the intersection of the curves. The  $r = 10$  mm radius size presented a good accuracy with the three types of filling pattern.

We can notice from the combination (material type, filling pattern), that nylon exhibited a lower accuracy with the three types of filling patterns compared to nylon reinforced carbon fiber and nylon reinforced glass fiber; the curves are practically linear which projects a weak correlation of the parameters and therefore a weak impact on the accuracy.

**Table 1** List of process variables and their levels

Factors	description	Level 1	Level 2	Level 3
A	Radius size	$r_1 = 5$ mm	$r_2 = 10$ mm	$r_3 = 15$ mm
B	Material Type	Nylon (polyamide 6)	Nylon (PA 6) + Carbon Fiber reinforcement	Nylon (PA 6) matrix + Glass Fiber reinforcement
C	Filling pattern	Triangular	Rectangular	Hexagonal

**Fig. 5** **a** Pareto chart of standardized effects for the average deviation, **b** main effects graph for the average deviation, and **c** interactions for the average deviation

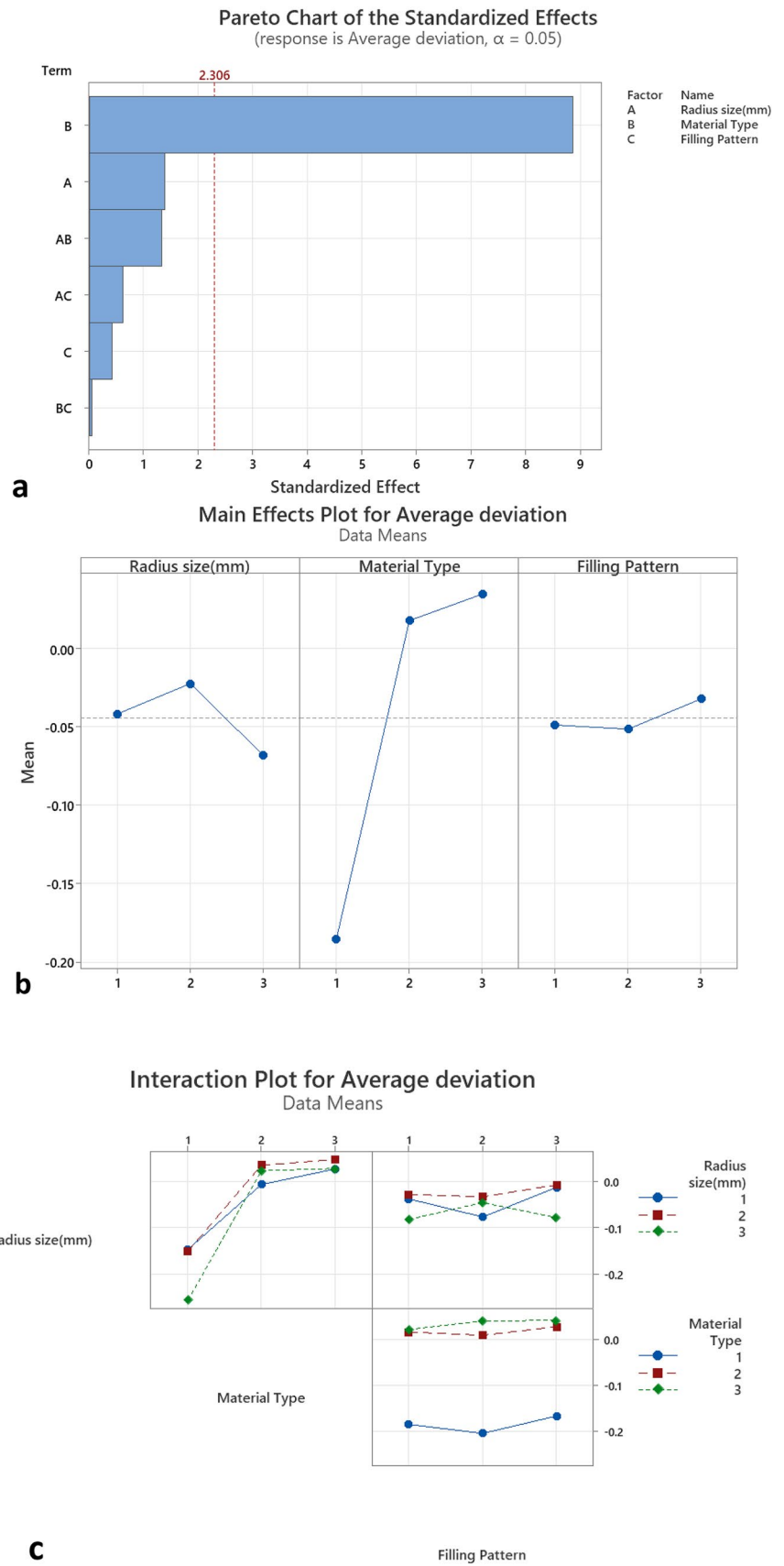


Figure 5 a Pareto chart of standardized effects for the average deviation, b Main effects graph for the average deviation, and c Interactions for the average deviation.

## 4.2 Analysis of the input factors on the variance

### 4.2.1 Analysis of the normalized effects of variance

The normalized effects are presented in Fig. 6 (a). The standardized effects of factors A, B, C and combinations AB, BC, AC, are less than 2.306, which means that these six factors and combinations have a small impact on the variance.

### 4.2.2 Main effects for the variance

Figure 6 (b) indicates that:

- The radiuses of 5 and 10 mm generate a small variance. The variance for the radius  $r = 15$  mm is significantly greater than that of the other radiuses. The larger the radius, the greater the dispersion.
- The variance for nylon material (PA6) is much higher than that of carbon reinforced material.
- The triangular and hexagonal filling pattern presented approximately the same variance; the rectangular filling pattern presented a small variance.

### 4.2.3 Interactions for the variance

The curves in Fig. 6 (c) show a cross-interaction between the three factors.

- The interaction between the parameters ‘radius size’ and ‘material type’ states that the maximum value of variance is reached with nylon for  $r = 15$  mm.
- For the nylon reinforced carbon material, the variance value is not affected by the radius size, for  $r = 5, 10$  and  $15$  mm the variance is very low.
- For the combination (radius, filling pattern), the triangular and rectangular filling patterns with the radius  $r = 5$  mm and  $r = 10$  mm show a variance that is very low; the radius of  $r = 15$  mm with triangular filling pattern reached a maximum variance value of 0.040. For the hexagonal filling pattern, the variance with the smallest radius  $r = 5$  mm size is almost null, and with slightly different values for radiuses  $r = 10$  mm and  $r = 15$  mm.
- The correlation results between the type of filling pattern and the material adopted differ according to the type of filling used. The variance is almost null for the nylon reinforced with carbon fiber with the three types of filling pattern. With the hexagonal filling pattern, the nylon and nylon reinforced with glass fiber both gave the same variance value, approximately 0.024.

## 5 Mathematical «elliptical» modelling of the printed part

In each section of the printed cylinder, the geometric measurement of Sect. 2.1.2 provides a set of  $N$  points with coordinates  $(R_i, \theta_i)$ ,  $1 \leq i \leq N$  in the local  $(r, \theta)$  plane. We make the assumption (not restrictive but which makes it possible to simplify the algorithms) that the angles  $\theta$  are distributed regularly on the circle, i.e.,  $\theta_i = (i-1) 2\pi/N$ . We are looking for an ellipse, centred on the origin of the coordinate system, passing as close as possible to these  $N$  points. More precisely, such an ellipse is characterized by the following equation in the  $(r, \theta)$  plane:

$$r(\theta) = \frac{a}{\left( \cos^2(\theta - \bar{\theta}) + \tau^2 \sin^2(\theta - \bar{\theta}) \right)^{1/2}}$$

where  $a$  represents the length of one of the semi-axes,  $\tau = \frac{a}{b}$  represents the aspect ratio of the two semi-axes ‘ $a$ ’ and ‘ $b$ ’ and finally  $\bar{\theta}$  is the inclination of the ellipse with respect to the horizontal axis: for  $k \in \mathbb{Z}$ , when  $\theta = \bar{\theta} + k\pi$  then the radius is ‘ $a$ ’, and when  $\theta = \bar{\theta} + \pi/2 + k\pi$  then the radius is ‘ $b$ ’. We take note that for a given ellipse, this representation is not unique: for  $k \in \mathbb{Z}$  we can arbitrarily add  $k\pi$  to  $\bar{\theta}$  without changing the expression of  $r$ .

The sequel of this section presents theoretical conditions and a practical algorithm allowing to find ‘ $a$ ’, ‘ $\tau$ ’ and ‘ $\bar{\theta}$ ’ such that the following quantity is minimal:

$$J(a, \tau, \bar{\theta}) = \sum_{i=1}^N [R_i - r(\theta_i)]^2 \quad (1)$$

Note that  $|R_i - r(\theta_i)|$  is not exactly the distance of the point  $(R_i, \theta_i)$  to the ellipse with equation  $\theta \rightarrow r(\theta)$  so we are not going to exactly find the “closest” ellipse in the sense of distances, but the ellipse which minimizes (1).

### 5.1 Obtaining a nonlinear system by writing first-order optimality conditions

By writing the first-order optimality conditions  $\frac{\partial J}{\partial a}(a, \tau, \bar{\theta}) = \frac{\partial J}{\partial \tau}(a, \tau, \bar{\theta}) = \frac{\partial J}{\partial \bar{\theta}}(a, \tau, \bar{\theta}) = 0$  and denoting:

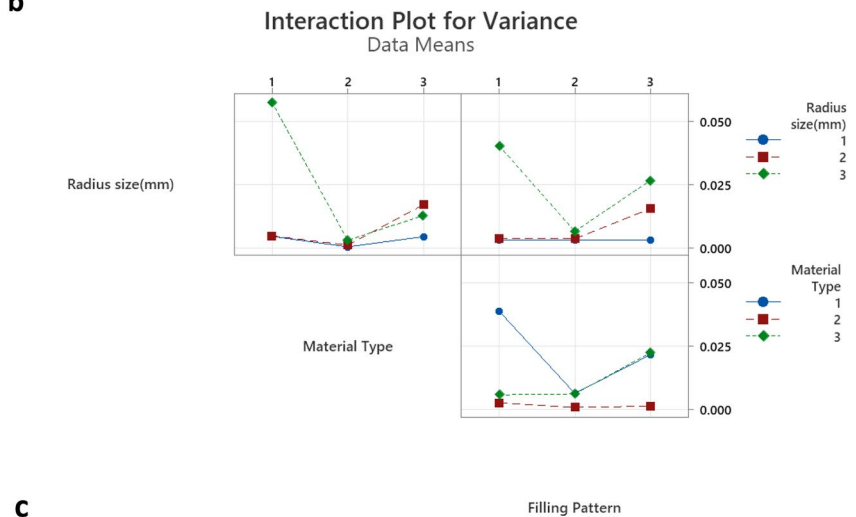
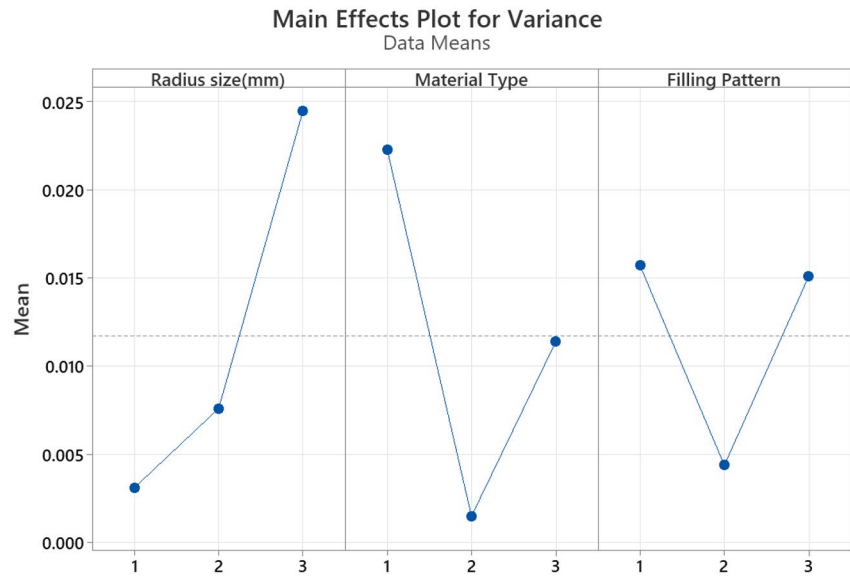
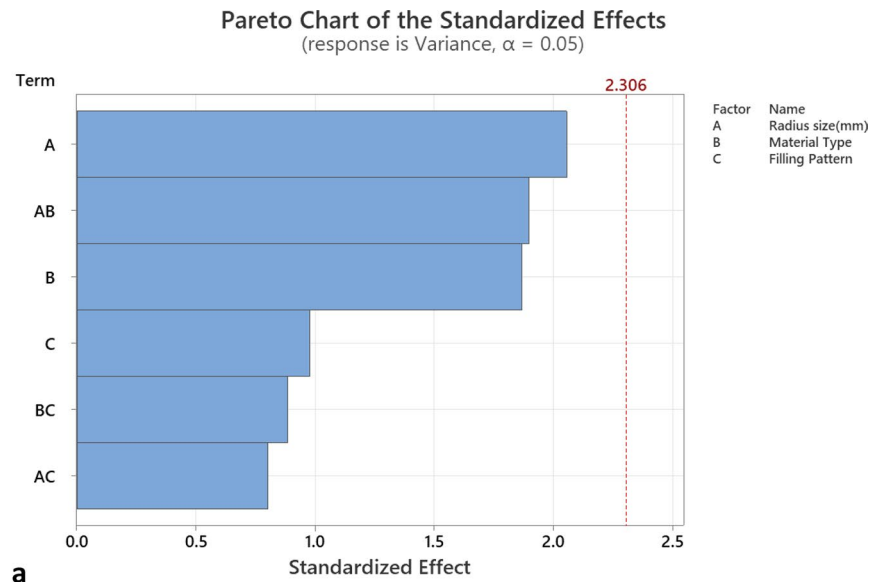
$$g_i = \left( \cos^2(\theta_i - \bar{\theta}) + \tau^2 \sin^2(\theta_i - \bar{\theta}) \right)^{1/2},$$

we get the following expressions:

$$-\frac{1}{2} \frac{\partial J}{\partial a}(a, \tau, \bar{\theta}) = \sum_{i=1}^N \left[ R_i - \frac{a}{g_i} \right] \frac{1}{g_i} = 0 \quad (2)$$



**Fig. 6** **a** Pareto chart of normalized effects for the variance, **b** Main effects plot for variance, **c** Interactions for variance



$$\left(\frac{1}{2\tau a}\right) \frac{\partial J}{\partial \tau}(a, \tau, \bar{\theta}) = \left[R_i - a/g_i\right] \left(\sin^2(\theta_i - \bar{\theta})\right) / g_i^3 = 0 \quad (3)$$

$$\frac{1}{a} \frac{\partial J}{\partial \bar{\theta}}(a, \tau, \bar{\theta}) = \sum_{i=1}^N \left[R_i - a/g_i\right] \left((1 - \tau^2) \sin(2\theta_i - \bar{\theta})\right) / g_i^3 \quad (4)$$

Eliminating  $a$  from the three equalities (2)-(3)-(4), we obtain the following (non-linear)  $2 \times 2$  system, whose unknowns are  $(\tau, \bar{\theta})$ :

$$\sum_{i=1}^N \frac{R_i}{g_i} \times \sum_{i=1}^N \frac{\sin^2(\theta - \bar{\theta})}{g_i^4} - \sum_{i=1}^N \frac{\sin^2(\theta - \bar{\theta})}{g_i^3} = 0 \quad (5)$$

$$\sum_{i=1}^N \frac{R_i}{g_i} \times \sum_{i=1}^N \frac{\sin(2(\theta - \bar{\theta}))}{g_i^4} - \sum_{i=1}^N \frac{\sin(2(\theta - \bar{\theta}))}{g_i^3} = 0 \quad (6)$$

## 5.2 Newton's algorithm for solving system (5)–(6)

System (5)–(6) is a non-linear system of two equations with two unknowns, which are  $\tau$  and  $\bar{\theta}$ . Once these values are found, we can calculate ' $a$ ' by any of the three expressions (2)–(4). Let  $F_1(\tau, \bar{\theta})$  be the function on the left-hand side of (5) and  $F_2(\tau, \bar{\theta})$  the function on the left-hand side of (6). Newton's algorithm applied to system (5)–(6) consists in generating a sequence  $(\tau_n, \bar{\theta}_n)_{n \geq 1}$  intended to converge towards a solution of the system. Let us list the three usual steps of Newton's algorithm.

### 5.2.1 Determining a starting point

As is well known, Newton's algorithm will converge if and only if its starting point is close enough to the solution. We opted for the following idea: we calculate the distance between the pairs of diametrically opposite points which are provided; the maximum of these values is a reasonable approximation of  $2a$  which is the major diameter of the ellipse, the angle corresponding to this couple of points is a reasonable approximation of  $\bar{\theta}$ , the distance between the two points obtained by a rotation of angle  $\pi/2$  is a reasonable approximation of  $2b$  which is the minor diameter of the ellipse.

### 5.2.2 Update

Let  $A(\tau_{n-1}, \bar{\theta}_{n-1})$  denote the Jacobian matrix of  $(F_1, F_2)$  in  $(\tau_{n-1}, \bar{\theta}_{n-1})$ :

$$A(\tau_{n-1}, \bar{\theta}_{n-1}) = \begin{pmatrix} \frac{\partial F_1}{\partial \tau}(\tau_{n-1}, \bar{\theta}_{n-1}) & \frac{\partial F_1}{\partial \bar{\theta}}(\tau_{n-1}, \bar{\theta}_{n-1}) \\ \frac{\partial F_2}{\partial \tau}(\tau_{n-1}, \bar{\theta}_{n-1}) & \frac{\partial F_2}{\partial \bar{\theta}}(\tau_{n-1}, \bar{\theta}_{n-1}) \end{pmatrix}$$

$$(\tau_n, \bar{\theta}_n) = (\tau_{n-1}, \bar{\theta}_{n-1}) - \left( A^{-1}(\tau_{n-1}, \bar{\theta}_{n-1}) \begin{pmatrix} F_1(\tau_{n-1}, \bar{\theta}_{n-1}) \\ F_2(\tau_{n-1}, \bar{\theta}_{n-1}) \end{pmatrix} \right)^T$$

The update is written

We have added a few safeguards to this standard process:

- The variable  $\tau$  being a ratio of two lengths, it must remain positive, which is not automatically provided by this update; if  $\tau_n < 0$  then we cancel the update of this variable:  $\tau_n = \tau_{n-1}$ ,
- we impose on the variable  $\tau_n$  not to exceed a limit value if the value of  $J$  (the function of (1)) evaluated at  $(a_n, \tau_n, \bar{\theta}_n)$  is greater than the previous value of  $J$  at  $(a_{n-1}, \tau_{n-1}, \bar{\theta}_{n-1})$ . This limit value can be adjusted if needed; we chose 20, value beyond which we can consider that the algorithm is diverging if moreover  $J$  has increased instead of diminishing. If  $\tau_n$  exceeds this limit value, we reset  $\tau_n$  to the value 1 (another value could be chosen).

### 5.2.3 Stopping test

These are two quite classic tests; we stop the updates when one of the following two criteria is met:

- Any norm of  $(F_1(\tau_n, \bar{\theta}_n), F_2(\tau_n, \bar{\theta}_n))$  is lower than a tolerance fixed by the user; if this criterion is met, then the algorithm has fulfilled its mission: find the couple  $(\tau, \bar{\theta})$  such that (5)–(6) is satisfied (up to the given tolerance).
- The number of iterations of the algorithm exceeds a threshold set by the user; if this criterion is met, then the algorithm has not fulfilled its mission; this safeguard is necessary so that the algorithm terminates if it does not converge.

This algorithm allows calculating the value of the major axis " $a$ ", the minor axis " $b$ " from which we deduce the departure from cylindricity  $c = |a - b|$ .

The results of departure from cylindricity calculation are presented in Table 2.

## 6 Conclusion

This study assesses and analyzes the effect of processing parameters including radius size, material type, and filling pattern on the dimensional accuracy from the design phase

**Table 2** The results of deviation from cylindricity calculation

	$r=5$ mm	$r=10$ mm	$r=15$ mm	$r=5$ mm	$r=10$ mm	$r=15$ mm	$r=5$ mm	$r=10$ mm	$r=15$ mm
	Triangular			Rectangular			Hexagonal		
Nylon	0.1075 mm	0.1184 mm	0.0949 mm	0.1014 mm	0.0946 mm	0.0998 mm	0.1 mm	0.1032 mm	0.096 mm
Nylon + Glass Fiber	0.0961 mm	0.1041 mm	0.1067 mm	0.0981 mm	0.1159 mm	0.0893 mm	0.0935 mm	0.1049 mm	0.1035 mm
Nylon + Carbon fiber	0.1097 mm	0.1137 mm	0.1016 mm	0.1112 mm	0.1086 mm	0.1301 mm	0.1045 mm	0.1068 mm	0.1153 mm

to the validation phase of components manufactured by the FFF process.

The results show that:

- The filling pattern type has no significant importance on precision for this study case. The material type affects dimensional accuracy the most.
- The 15 mm radius exhibited the greatest inaccuracy compared to 5 and 10 mm sizes, which means that the bigger the part, the lower the dimensional accuracy.
- The glass fiber reinforced nylon ranked as the best material type with lower dimensional inaccuracy compared to nylon reinforced carbon fiber and nylon.

The modelling of the actual printed parts allows characterizing each section (layer) as an ellipse; the algorithm allows calculating the value of the major axis and the minor axis from which we deduce the deviation from cylindricity.

The low variance indicates that the machine is repetitive and, therefore, it is meaningful to attempt to correct printing errors.

The work of identifying the influence of factors will allow in the future analysis work to focus on the most influential. For better accuracy in 3D printing, the simplified method of correction of input parameters will be even more relevant. Once this correction process is implemented for a given printer, repetition of experiments for the same sets of parts will be needed in order to evaluate the associated tolerance ranges.

## Appendix

**The experimental design matrix, an L9 ( $3^3$ ), with 27 runs was chosen to account for the factors and their levels (Table 3).**

**Table 3** The DOE matrix for the factors and their levels

Trials	Radius size(mm)	Material type	Filling pattern	Variance	Average deviation
1	1	1	1	0.0036	−0.102
2	1	2	1	0.0006	−0.0124
3	1	3	1	0.0049	0.003
4	1	1	2	0.0052	−0.258
5	1	2	2	0.0002	−0.012
6	1	3	2	0.0040	0.041
7	1	1	3	0.0048	−0.081
8	1	2	3	0.0004	0.0059
9	1	3	3	0.0043	0.039
10	2	1	1	0.0050	−0.143
11	2	2	1	0.0013	0.0353
12	2	3	1	0.0051	0.0245
13	2	1	2	0.0046	−0.160
14	2	2	2	0.0011	0.030
15	2	3	2	0.0049	0.032
16	2	1	3	0.0046	−0.150
17	2	2	3	0.0009	0.042
18	2	3	3	0.041	0.0875
19	3	1	1	0.1081	−0.309
20	3	2	1	0.0056	0.026
21	3	3	1	0.0071	0.038
22	3	1	2	0.0091	−0.195
23	3	2	2	0.001	0.01
24	3	3	2	0.0094	0.049
25	3	1	3	0.0555	−0.268
26	3	2	3	0.0024	0.0357
27	3	3	3	0.0219	−0.001

**ANOVA report for average deviation****Analysis of variance**

See Table 4.

**Table 4** Analysis of variance

Source	DF	Adj SS	Adj MS	F Value	P Value
Model	18	0.307867	0.017104	7.02	0.004
Linear	6	0.280965	0.046828	19.21	0.000
Radius size(mm)	2	0.009531	0.004766	1.95	0.204
Material type	2	0.269474	0.134737	55.27	0.000
Filling pattern	2	0.001960	0.000980	0.40	0.682
2-Way interactions	12	0.026902	0.002242	0.92	0.568
Radius size(mm)*material type	4	0.017556	0.004389	1.80	0.222
Radius size(mm)*filling pattern	4	0.007857	0.001964	0.81	0.555
Material type*filling pattern	4	0.001489	0.000372	0.15	0.956
Error	8	0.019503	0.002438		
Total	26	0.327370			

**Model summary**

See Table 5

**Table 5** Model summary of variance

S	R-sq	R-sq(adj)	R-sq(pred)
0.0493743	94.04%	80.64%	32.14%

**Coefficients**

See Table 6

**Table 6** Coefficients of variance

Term	Coef	SE Coef	T Value	P Value	VIF
Constant	−0.04417	0.00950	−4.65	0.002	
Radius size(mm)					
1	0.0023	0.0134	0.17	0.866	1.33
2	0.0218	0.0134	1.62	0.144	1.33
Material type					
1	−0.1409	0.0134	−10.49	0.000	1.33
2	0.0620	0.0134	4.61	0.002	1.33
Filling pattern					
1	−0.0047	0.0134	−0.35	0.737	1.33
2	−0.0073	0.0134	−0.54	0.603	1.33
Radius size(mm)*material type					
1 1	0.0358	0.0190	1.88	0.097	1.78
1 2	−0.0263	0.0190	−1.39	0.203	1.78
2 1	0.0124	0.0190	0.65	0.534	1.78
2 2	−0.0038	0.0190	−0.20	0.846	1.78
Radius size(mm)*filling pattern					
1 1	0.0094	0.0190	0.49	0.635	1.78
1 2	−0.0272	0.0190	−1.43	0.190	1.78
2 1	−0.0006	0.0190	−0.03	0.974	1.78
2 2	−0.0030	0.0190	−0.16	0.879	1.78
Material type*filling pattern					
1 1	0.0051	0.0190	0.27	0.794	1.78
1 2	−0.0119	0.0190	−0.63	0.547	1.78
2 1	0.0031	0.0190	0.17	0.873	1.78
2 2	−0.0012	0.0190	−0.06	0.950	1.78

## ANOVA report for variance

### Analysis of variance

See Table 7

**Table 7** Analysis of variance for variance

Source	DF	Adj SS	Adj MS	F Value	P Value
Model	18	0.011234	0.000624	2.01	0.158
Linear	6	0.004951	0.000825	2.66	0.101
Radius size(mm)	2	0.002279	0.001139	3.67	0.074
Material type	2	0.001944	0.000972	3.13	0.099
Filling pattern	2	0.000728	0.000364	1.17	0.357
2 Way interactions	12	0.006283	0.000524	1.69	0.233
Radius size(mm)*material type	4	0.003583	0.000896	2.89	0.094
Radius size(mm)*filling pattern	4	0.001283	0.000321	1.03	0.446
Material type*filling pattern	4	0.001417	0.000354	1.14	0.403
Error	8	0.002483	0.000310		
Total	26	0.013717			

### Model summary

See Table 8

**Table 8** Model summary for variance

S	R-sq	R-sq(adj)	R-sq(pred)
0.0176162	81.90%	41.18%	0.00%

### Coefficients

See Table 9

**Table 9** Coefficients for variance

Term	Coef	SE Coef	T-Value	P-Value	VIF
Constant	0.01173	0.00339	3.46	0.009	
Radius size(mm)					
1	−0.00861	0.00479	−1.80	0.110	1.33
2	−0.00411	0.00479	−0.86	0.416	1.33
Material type					
1	0.01055	0.00479	2.20	0.059	1.33
2	−0.01023	0.00479	−2.13	0.066	1.33
Filling pattern					
1	0.00397	0.00479	0.83	0.431	1.33
2	−0.00734	0.00479	−1.53	0.164	1.33
Radius size(mm)*material type					
1 1	−0.00913	0.00678	−1.35	0.215	1.78
1 2	0.00751	0.00678	1.11	0.300	1.78
2 1	−0.01343	0.00678	−1.98	0.083	1.78
2 2	0.00371	0.00678	0.55	0.599	1.78
Radius size(mm)*filling pattern					
1 1	−0.00405	0.00678	−0.60	0.567	1.78
1 2	0.00736	0.00678	1.09	0.309	1.78
2 1	−0.00779	0.00678	−1.15	0.284	1.78
2 2	0.00326	0.00678	0.48	0.644	1.78
Material type*filling pattern					
1 1	0.01265	0.00678	1.87	0.099	1.78
1 2	−0.00864	0.00678	−1.27	0.238	1.78
2 1	−0.00297	0.00678	−0.44	0.673	1.78
2 2	0.00660	0.00678	0.97	0.359	1.78



**Funding** The authors declare that no funds, grants, or other support were received during the preparation of this manuscript.

**Data availability** The experimental part was carried out in the Product Design and Innovation laboratory of the National School of Arts et Metiers. The materials used were the Mark Two™ Markforged® 3D printer, the Solutionix D500 3D Scanner, and the Geomagic® Control X™ software to recover the data of dimensional comparison between the designed part and the 3D printed model.

**Code availability** Not applicable.

## Declarations

**Conflicts of interest** I hereby declare that all the authors of this work have no relevant financial or non-financial interests to disclose.

**Ethical approval** Not applicable.

**Consent to participate** Not applicable.

## References

- Huang Y, Leu MC, Mazumder J, Donmez A (2015) Additive manufacturing: current state, future potential, gaps and needs, and recommendations. *ASME J Manuf Sci Eng* 137(1):014001. <https://doi.org/10.1115/1.4028725>
- Kruth JP, Leu MC, Nakagawa T (1998) Progress in additive manufacturing and rapid prototyping. *CIRP Ann Manuf Technol* 47(2):525–540. [https://doi.org/10.1016/s0007-8506\(07\)63240-5](https://doi.org/10.1016/s0007-8506(07)63240-5)
- Levy GN, Schindel R, Kruth JP (2003) Rapid manufacturing and rapid tooling with layer manufacturing (LM) technologies, state of the art and future perspectives 2003. *CIRP Ann Manuf Technol* 52(2):589–609. [https://doi.org/10.1016/s0007-8506\(07\)60206-6](https://doi.org/10.1016/s0007-8506(07)60206-6)
- Chua CK, Leong KF (2015) 3D printing and additive manufacturing: principles and applications, fourth edition of rapid prototyping, 978–981. World Scientific Publishing Company, ISBN
- Adanur S, Jayswal A (2021) Additive manufacturing of interlaced fibrous structures. *J Rapid Prototyp* 27(4):671–681. <https://doi.org/10.1108/rpj-05-2020-0095>
- Melnikova R, Ehrmann A, Finsterbusch K (2014) 3D printing of textile-based structures by fused deposition modelling (FDM) with different polymer materials. *IOP Confer Series Mater Sci Eng*. 62:012018. <https://doi.org/10.1088/1757-899x/62/1/012018>
- Quan Z, Wu A, Keefe M, Qin X, Yu J, Suhr J, B, JH, Kim BS, Chou TW, (2015) Additive manufacturing of multi-directional preforms for composites: opportunities and challenges. *Mater Today* 18(9):503–512. <https://doi.org/10.1016/j.mattod.2015.05.001>
- Wohlers Associates (2013) Additive Manufacturing and 3D Printing State of the Industry. Wohlers Associates, Fort Collins, CO, Wohlers Report
- Jayswal A, Adanur S (2022) Effect of heat treatment on crystallinity and mechanical properties of flexible structures 3D printed with fused deposition modeling (2022). *J Ind Text* 51(2):2616S–2641S. <https://doi.org/10.1177/15280837211064937>
- Dommati H, Ray SS, Wang JC, Chen SS (2019) A comprehensive review of recent developments in 3D printing technique for ceramic membrane fabrication for water purification. *RSC Adv*. <https://doi.org/10.1039/c9ra00872a>
- Afrose MF, Masood SH, Iovenitti P, Nikzad M, Sbarski I (2016) Effects of part build orientations on fatigue behaviour of FDM-processed PLA material. *Prog Addit Manuf* 1:21–28. <https://doi.org/10.1007/s40964-015-0002-3>
- Yao SS, Jin FL, Rhee KY, Hui D, Park SJ (2017) Recent advances in carbon fiber reinforced thermoplastic composites: a review. *Composit Part B*. 142(2018):241–250. <https://doi.org/10.1016/j.compositesb.2017.12.007>
- Sobha AP, Sreekala PS, Narayanankutty SK (2017) Electrical, thermal, mechanical and electromagnetic interference shielding properties of PANI/FMWCNT/TPU composites. *Prog Org Coat* 113:168–174. <https://doi.org/10.1016/j.porgcoat.2017.09.001>
- Melenka GW, Cheung BKO, Schofield JS, Dawson MR, Carey JP (2016) Evaluation and prediction of the tensile properties of continuous fiber-reinforced 3D printed structures. *Compos Struct* 153(2016):866–875. <https://doi.org/10.1016/j.compstruct.2016.07.018>
- Dickson AN, Barry JN, McDonnell KA, Dowling DP (2017) Fabrication of continuous carbon, glass and kevlar fibre reinforced polymer composites using additive manufacturing. *Addit Manuf* 16:146–152. <https://doi.org/10.1016/j.addma.2017.06.004>
- Justo J, Tavarra K, Garcia-Guzman L, Paris F (2017) Characterization of 3D printed long fibre reinforced composites. *Compos Struct* 185(2018):537–548. <https://doi.org/10.1016/j.compstruct.2017.11.052>
- Omar Ahmed M, Syed Hasan M, Jahar Lal B (2015) Experimental investigations of process parameters influence on rheological behaviour and dynamic mechanical properties of FDM manufactured parts. *J Thermoplast Compos Mater* 31(15):1983–1994. <https://doi.org/10.1080/10426914.2015.1127955>
- Fernandez-Vicente M, Calle W, Ferrandiz S, Conejero A (2016) Effect of infill parameters on tensile mechanical behavior in desktop 3D printing. *3D Print Add Manuf*. 3(3):183–192. <https://doi.org/10.1089/3dp.2015.0036>
- Baich L, Manogharan G, Marie H (2015) Study of infill print design on production cost-time of 3D printed ABS parts. *Int J Rapid Manuf* 5(3–4):308–319. <https://doi.org/10.1504/IJRAPIDM.2015.074809>
- Akhoundi B, Behraves AH (2019) Effect of filling pattern on the tensile and flexural mechanical properties of FDM 3D printed products. *Exp Mech*. <https://doi.org/10.1007/s11340-018-00467-y>
- Maurya S, Malik B, Sharma P (2022) Investigation of different parameters of cube printed using PLA by FDM 3D printer. *Mater Today*. <https://doi.org/10.1016/j.matpr.2022.03.700>
- Alafaghania A, Qattawia A, Alrawia B, Guzman A (2017) A experimental optimization of fused deposition modelling processing parameters: a design-for-manufacturing approach. *Procedia Manuf* 10(2017):791–803. <https://doi.org/10.1016/j.promfg.2017.07.079>
- Gibson I, Rosen D, Stucker B (2010) Additive manufacturing technologies rapid prototyping to direct digital manufacturing. Springer, Boston, MA
- Jiang L, Ye H, Zhou C, Chen S, Xu W (2017) Parametric topology optimization toward rational design and efficient prefabrication for additive manufacturing. *J Manuf Sci Eng*. <https://doi.org/10.1115/1.5000000>
- Sood A, Ohdar R, Mahapatra S (2009) Improving dimensional accuracy of fused deposition modeling processed part using grey taguchi method *Mater*, 2009. *Des Mater Des* 30(2009):4243–4252. <https://doi.org/10.1016/j.mates.2009.04.030>
- Huang Y, Leu MC, Mazumder J, Donmez A (2015) Additive manufacturing: current state, future potential, gaps and needs, and recommendations. *J Manuf Sci Eng* 137(1):14001. <https://doi.org/10.1115/1.4028725>

27. Aboutaleb AM, Tschopp MA, Rao PK, Bian L (2017) Multi-objective accelerated process optimization of part geometric accuracy in additive manufacturing. *J Manuf Sci Eng.* <https://doi.org/10.1115/1.4037319>
28. Mahesh M, Wong Y, Fuh J, Loh H (2004) Benchmarking for comparative evaluation of rp systems and processes. *Rapid Prototyp J* 10(2):123–135. <https://doi.org/10.1108/13552540410526999>
29. Kruth JP (1991) Material increment manufacturing by rapid prototyping techniques. *CIRP Ann* 40:603–614. [https://doi.org/10.1016/S0007-8506\(07\)61136-6](https://doi.org/10.1016/S0007-8506(07)61136-6)
30. Bochmann L, Bayley C, Helu M, Transchel R, Wegener K, Dornfeld D (2015) Understanding error generation in fused deposition modeling. *Surf Topogr Metrol Prop* 3:014002
31. Mahesh M, Wong YS, Fuh JYH, Loh HT (2004) Benchmarking for comparative evaluation of RP systems and processes. *Rapid Prototyp. J.* 10(2):123135. <https://doi.org/10.1108/13552540410526999>
32. Weheba G, Sanchez-Marsa A (2006) Using response surface methodology to optimize the stereolithography process. *Rapid Prototyp J* 12(2):72–77. <https://doi.org/10.1108/13552540610652401>
33. El-Katatny I, Masood SH, Morsi YS (2010) Error analysis of FDM fabricated medical replicas. *Rapid Prototyping J* 16(1):36–43. <https://doi.org/10.1108/13552541011011695>
34. Tootooni MS, Dsouza A, Donovan R, Rao P, Kong Z, Borgesen P (2017) Assessing the geometric integrity of additive manufactured parts from point cloud data using spectral graph theoretic sparse representation-based classification. *ASME Paper No.* <https://doi.org/10.1115/MSEC2017-2794>
35. Tootooni MS, Dsouza A, Donovan R, Rao P, Kong Z, Borgesen P (2017) Classifying the dimensional variation in additive manufactured parts from laser-scanned three-dimensional point cloud data using machine learning approaches. *ASME J. Manuf. Sci. Eng.* 139(9):091005. <https://doi.org/10.1115/1.4036641>
36. Rao PK, Kong Z, Duty CE, Smith RJ, Kunc V, Love LJ (2015) Assessment of dimensional integrity and spatial defect localization in additive manufacturing using spectral graph theory. *ASME J. Manuf. Sci. Eng.* 138(5):051007. <https://doi.org/10.1115/1.4031574>
37. Garg N, Rastogi V, Kumar P (2022) Process parameter optimization on the dimensional accuracy of additive manufacture Thermoplastic Polyurethane (TPU) using RSM. *Today. Proc. Mater.* <https://doi.org/10.1016/j.matpr.2022.02.309>
38. Borouchaki H, Frey PJ (2022) Simplification of surface mesh using Hausdorff envelope. *Comput. Methods Appl. Mech. Engrg.* 15(194):48–49. <https://doi.org/10.1016/j.cma.2004.11.016>
39. Véron P, Léon JC (1997) Static polyhedron simplification using error measurements. *Aided Geom. Des. Comp.* [https://doi.org/10.1016/S0010-4485\(96\)00057-7](https://doi.org/10.1016/S0010-4485(96)00057-7)
40. H Borouchakiet et al. 1997 Maillage géométrique de surfaces. Partie II: appauvrissement RR-INRIA
41. Frey PJ, Borouchaki H (2003) Surface meshing using a geometric error estimate. *J. Numer. Methods Engrg. Int.* <https://doi.org/10.1002/nme.766>
42. Escobar JM, Cascón JM, Rodríguez E, Montenegro R (2011) A new approach to solid modeling with trivariate T-splines based on mesh optimization. *Comput Methods Appl Mech Engrg* 200:3210–3222. <https://doi.org/10.1016/j.cma.2011.07.004.2011>
43. Dantan JY, Huang Z, Goka E (2017) Geometrical variations management for additive manufactured product. *CIRP Ann Manuf Technol* 66:161–164162. <https://doi.org/10.1016/j.cirp.2017.04.034>
44. Franco P, Sanchez MT, Nalda E (2021) Mathematical models for the dimensional accuracy of products generated by additive manufacturing. *Adv Math for Industry.* Elsevier., Amsterdam Netherland, pp 361–388
45. Zhu Z, Keimasi S, Anwer N, Mathieu L, Qiao L (2017) review of shape deviation modeling for additive manufacturing. *Advanc Mech Desig Eng Manufact Lectur Note Mech Eng.* [https://doi.org/10.1007/978-3-319-45781-9\\_25](https://doi.org/10.1007/978-3-319-45781-9_25)
46. Mohamed OA, Masood SH, Bhowmik JL (2015) Optimization of fused deposition modeling process parameters: a review of current research and prospects. *Adv Manuf* 3(1):42–53. <https://doi.org/10.1007/s40436-014-0097-7>
47. Gebhardt A (2012) Understanding Additive Manufacturing. ISBN 978–3–446–42552–1 E-Book-ISBN 978–3–446–43162–1
48. Minitab17. [https://www.minitab.com/uploadedfiles/Documents/gettingstarted/Minitab17\\_gettingstarted-en.pdf](https://www.minitab.com/uploadedfiles/Documents/gettingstarted/Minitab17_gettingstarted-en.pdf).

**Publisher's Note** Springer Nature remains neutral with regard to jurisdictional claims in published maps and institutional affiliations.

Springer Nature or its licensor (e.g. a society or other partner) holds exclusive rights to this article under a publishing agreement with the author(s) or other rightsholder(s); author self-archiving of the accepted manuscript version of this article is solely governed by the terms of such publishing agreement and applicable law.